

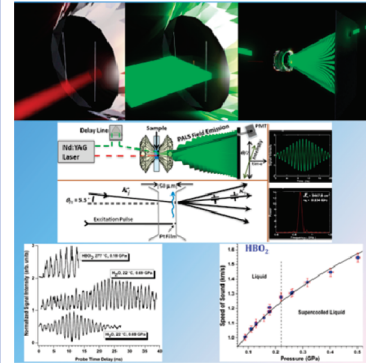
Photoacoustically Measured Speeds of Sound of Liquid HBO₂: Semi-Empirical Modeling of Boron-Containing Explosives

Joseph M. Zaug,* Sorin Bastea, Jonathan C. Crowhurst, Michael R. Armstrong, and Nick E. Teslich, Jr.

Lawrence Livermore National Laboratory, Physical and Life Sciences, P.O. Box 808, L-350, Livermore, California 94551

ABSTRACT Elucidation of geodynamic, geochemical, and shock-induced processes is often limited by challenges to determine accurately molecular fluid equations of state (EOS). High-pressure liquid-state reactions of carbon species underlie physicochemical mechanisms such as differentiation of planetary interiors, deep carbon sequestration, propellant deflagration, and shock chemistry. Here we introduce a versatile photoacoustic technique developed to measure precise adiabatic speeds of sound of high-pressure molecular fluids and fluid mixtures. Metaboric acid, HBO₂ speeds of sound are measured up to 0.5 GPa along the 277 °C isotherm. A polarized Exponential-6 interatomic potential form, parameterized using our data, enables EOS determinations and corresponding semiempirical evaluations of > 2000 °C thermodynamic states including energy release from bororganic formulations. Our thermochemical model predictions of boronated hydrocarbon shock Hugoniot states differ from experiment by < 3%.

SECTION Energy Conversion and Storage



Fluid state high-pressure and temperature physicochemical processes involving metallic and carbon-containing reactants are common in nature and command the interests of a wide range of interdisciplinary and technological endeavors (astro, planetary, geo, and atmospheric sciences; nuclear engineering; combustion, propellant, and high explosive materials science; and explosive crystallization and welding of technologically important materials to name but just a few).^{1–9} Quantitative predictions of extreme-condition chemistry are inexorably linked to knowing EOS of probable major reaction species. For example, the optimal use of metal fuel additives to enhance the release of chemical energy stored in organic crystals has been hindered by the lack of oxide component EOS data. Aluminum (Al) powder has long been proposed as a promising candidate fuel to increase chemical power output of highly energetic (HE) material formulations significantly.⁸ Large-scale tests revealed that Al additives actually decrease shock pressure and reaction velocities of HEs, an effect later attributed to low heat of formation oxide products at the Chapman–Jouguet (C–J) state of explosives (the thermodynamic state where reaction products behind a steady propagating detonation wave reach chemical equilibrium).⁶ It is now well understood that exothermic reactions must meet or exceed high melt temperatures of metal oxides before fuel enhancement can be achieved. Inability to realize the full potential of Al fuel lead to consideration of utilizing boron, which has the highest elemental heat of combustion per unit volume, $\Delta H = 137.45 \text{ kJ/cc}$.⁹ Combustion enhancement using boron has also proved to be

difficult to harness; the complete oxidation of boron can be poisoned by the presence of a common reaction product, water vapor.¹⁰ To elucidate sufficiently the chemical energy landscape of metalized propellants or HEs, the efficacy of controlled parameters, for example, metal powder grain size and concentration, pure metal powder or metal fractionated compounds, oxidizer and fluorinator concentration, and so on, continue to be examined using combustion or large-scale tests. Macroscopic-scale performance metrics of tested formulations such as energy release and reaction rate provide the necessary information required to challenge predictions made using EOS-based thermochemical models. Therefore, stringently refined semiempirical computational models serve to guide and reduce time-consuming and dangerous investigations of new formulations.

Studies of combustion of boron-containing systems indicate that a simple molecular product, HBO₂, significantly affects the energy output because it is an effective molecular trap to boron on its path to full oxidation.¹¹ We hypothesize that HBO₂ will likely have a similar effect on the properties of boron-containing HEs. Despite decades of study, however, there are no HBO₂ EOS-type data available to test such predictions. In this Letter, we present the first such experimental results on the sound velocity, c , of HBO₂ at elevated pressures and temperatures. Normally we apply the impulsive

Received Date: May 20, 2010

Accepted Date: September 15, 2010

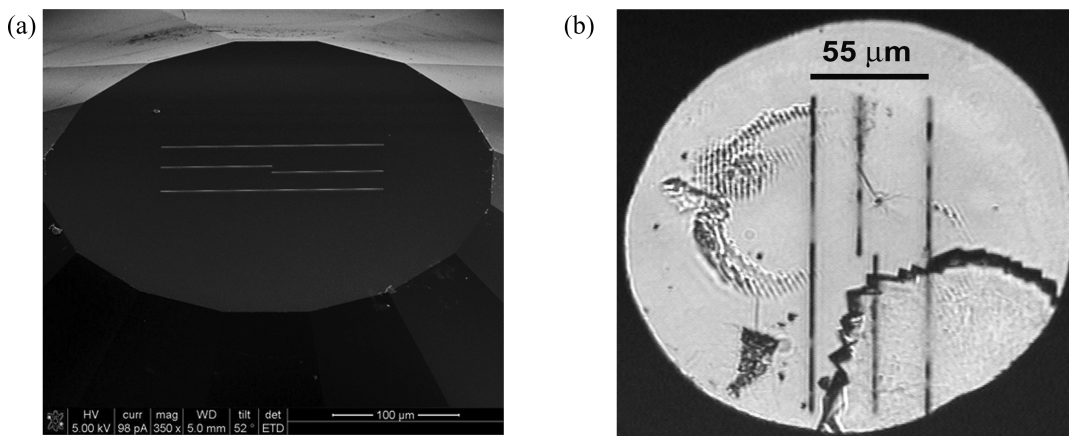


Figure 1. (a) SEM image of platinum strips deposited onto a diamond-anvil. (b) Photomicrograph of a DAC sample chamber. At 0.4 GPa and 277 °C, solid HBO₂, lower right region, slowly encroaches on the supercooled fluid. Inspection of the left side of the chamber reveals gratings that were burned into the culet from failed attempts to generate traditional ISLS signals. A SrB₄O₇:Sm²⁺ optical pressure manometer rests below the gratings in the 7 o'clock region of the chamber.

stimulated light scattering (ISLS) technique to generate and probe acoustic wave propagation in fluid samples encapsulated within resistively heated diamond-anvil cells (DACs).^{12–14} However, there are practical limitations to the ISLS technique applied to optically and physically thin fluids: they must minimally absorb excitation-pulse light and, exhibit no photo reactions with either excitation- or probe-pulses. Also, the diffractive strength of a sample scales with physical thickness. Unfortunately, HBO₂(liq.) did not absorb the fundamental or higher harmonics of our 1064 nm excitation source. Furthermore, we observe a high propensity for HBO₂ (solid) photochemistry induced by overlapped ISLS excitation pulses (1.0 to 1.4 GW/cm² peak Gaussian profile irradiance) and also by a 1–5 mW 488 nm continuous wave (CW) Raman and fluorescence probe (1.2–6.4 kW/cm² local irradiance).

In this Letter, we introduce a laser-based time-domain (T-D) variation of well-established photoacoustic light scattering techniques to enable *in situ* sound velocity measurements of physically or optically thin materials encapsulated under nonambient pressure–temperature conditions; for the sake of brevity, we will use the acronym PALS to indicate photoacoustic light scattering. In this variation, a metal strip absorbs a short pulse of laser light and then functions as a transducer to launch a broadband pulse into the surrounding medium laterally. When the transducer is then struck by a second optical pulse, it passively generates local oscillator (LO) signal. Speeds of sound can then be measured downstream from the sample container using the heterodyne detection method. (See below.) Once a suitable wavevector is established, the accuracy of the PALS measurement is quantified by comparison of published H₂O (liquid) and H₂O (solid) sound velocity results; in turn, HBO₂(liq.) results are measured to establish an EOS. The PALS approach has several advantages: (1) low average irradiance, between one and three orders of magnitude less than conventional laser-based sound velocity measurement techniques, which significantly reduces the potential for photochemical reactions; (2) inherently low frequency measurements (approximately 0.5–5.0 GHz for fluids or

5–20 times lower than frequency-domain measurements when applied to high-pressure fluids), which help to avoid or minimize liquid-state acoustic dispersion effects; (3) easily characterized acoustic dispersion, which can be conducted by symmetrically changing the incident and selected scattering wavevector of the probe beam, thus allowing determination of structural relaxation rates of polymers or glassy-like materials; (4) material index is not required to determine *c*; and (5) permits the study of physically thin materials, for example, <5 μm. The technical advantages of using T-D techniques for the study of fluids have been previously discussed.¹² Here we provide sound velocity data from a material that is highly susceptible to laser-induced photochemistry.

A PALS transducer is made by first depositing a platinum strip onto the culet of a diamond-anvil using a focused ion beam. (See the Supporting Information.) The line width is 0.5 to 1.0 μm, and the thickness is 0.27 μm or approximately one-half of the probe wavelength value. Initially, four lines of varying separation were deposited onto culets to obtain a sufficient number of acoustic fringes for either slow or fast propagation velocities: narrow separations for slow wave propagation speeds and wide separations for faster propagation speeds (Figure 1). To generate sound, a 100 ps optical pulse is focused onto a Pt strip; see Figure 2. The peak laser irradiance, <0.03 GW/cm², impulsively increases temperature in the transducer (electron–phonon energy transfer) by a few degrees. The temperature increase produces a thermal stress distribution in the Pt region struck by the laser pulse, which then launches a longitudinal strain-pulse. The pulse energy is reflected and transmitted at the interface between the strip and the surrounding sample. Transmitted broadband pulses that travel perpendicular to the direction of the excitation-pulse and into the surrounding medium are utilized to make sound velocity determinations. Two different pump and probe beam configurations are shown in Figure 3a. We emphasize that the physics behind similar photoacoustic transducers, for example, back scattering geometries, is well-documented, however the geometry and application of

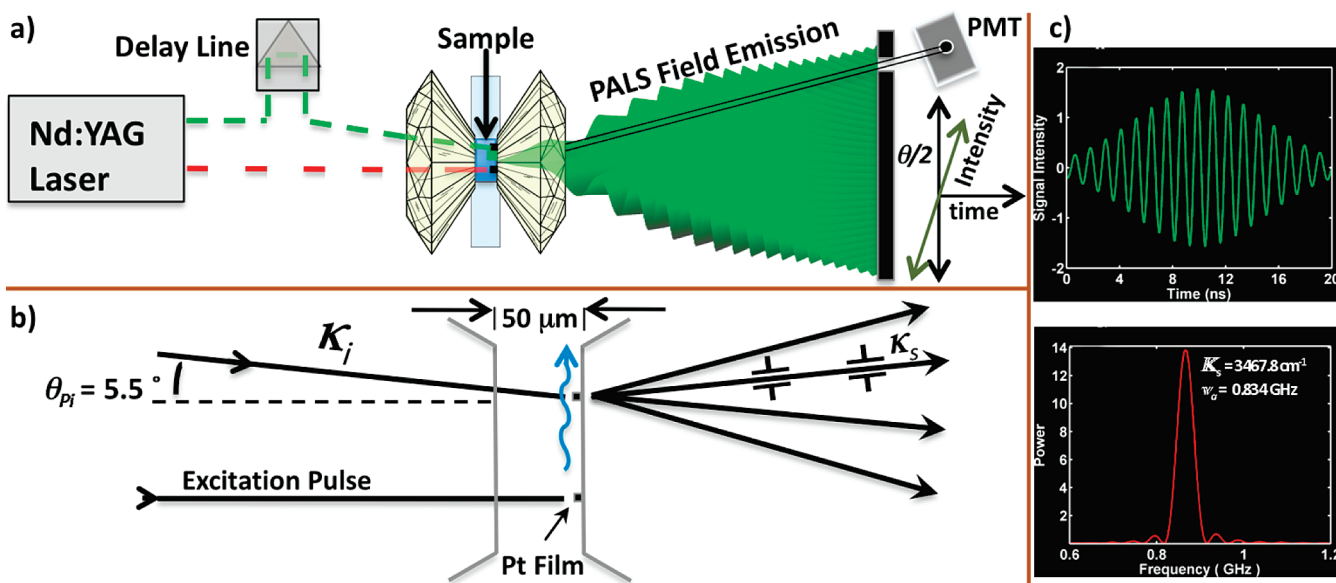


Figure 2. (a) PALS is initiated when a fwhm 100 ps 1064 nm laser pulse (red dashed line) strikes a Pt strip deposited onto a diamond culet. The strip subsequently launches a broadband acoustic pulse. A time-of-flight delayed train of probe pulses (532 nm, green dashed line) diffracts from a second Pt strip and the traveling acoustic wavefront. Two apertures pass both diffracted signals along a selected wavevector, K_s , to a photomultiplier tube, where they mix. (b) Schematic diagram showing several available wavevectors, including K_s , at a point in time when the acoustic wave crosses the second Pt strip. (c) PALS time series is Fourier transformed to determine acoustic frequency, ν_A ; $c = \nu_A/K_s$. Here the time series and power spectrum are calculated from an analytically computed PALS field emission (green colored fan drawn in part a), which represents a continuous 20 ns signal from water at 22 °C and 0.66 GPa. The analytical expression derived to compute emission, $\nu_A = 2cl_p (\sin \theta/2)$, describes a propagating diffraction plane, with velocity = c ; wavevector conservation is maintained. (See below.) A Gaussian window is used to match the emission intensity observed by two Pt strip data; see Figure 3b.

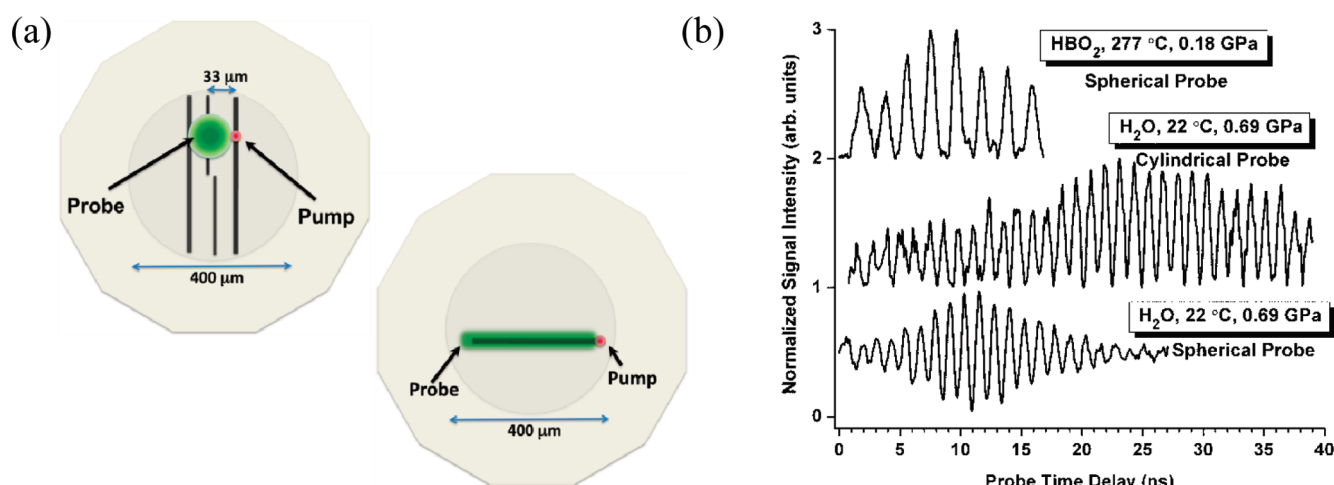


Figure 3. (a) Schematic diagram of Pt strip configurations proven suitable for either spherically or cylindrically focused probe beams. Experiments were conducted using a nominal full width half-maximum pump-pulse spot size of 10 μm . The single strip configuration is more optimal to use than the original multistrip design. (b) PALS time-domain traces from liquid H_2O and HBO_2 .

our device is unique.^{15–18} At 277 °C and 0.01 GPa, the acoustic impedance of Pt $\approx 8.8 \times 10^7 \text{ kg/s} \cdot \text{m}^2$ and HBO_2 (liq.) $= 6.5 \times 10^5 \text{ kg/s} \cdot \text{m}^2$. The transmitted acoustic intensity, I_T , at 0.01 GPa is 2.9%. In general, I_T will increase with applied pressure because fluids are more compressible than metal; for example, $I_T \approx 4.2\%$ at 0.5 GPa. The traveling acoustic peak (expansion of the medium) increases and the acoustic trench (rarefaction following expansion of the medium) reduces the nominal index of refraction of the sample and therefore alters

the local magnitude of optical diffraction. A time-of-flight delayed 532 nm probe-pulse ($\sim 20 \mu\text{m}$ fwhm spot size) is focused onto a second and parallel Pt strip. Each T-D datum point represents the average of at least 800 laser shots, and each time series is 500–800 points in length. A CW laser probe and a sufficiently fast photodetector and oscilloscope could be employed to collect an entire T-D series in real-time. Probe radiation scatters off of Pt strips, forming a LO or reference field, E_R , ($I_R = E_R^2$), with a constant phase. Probe

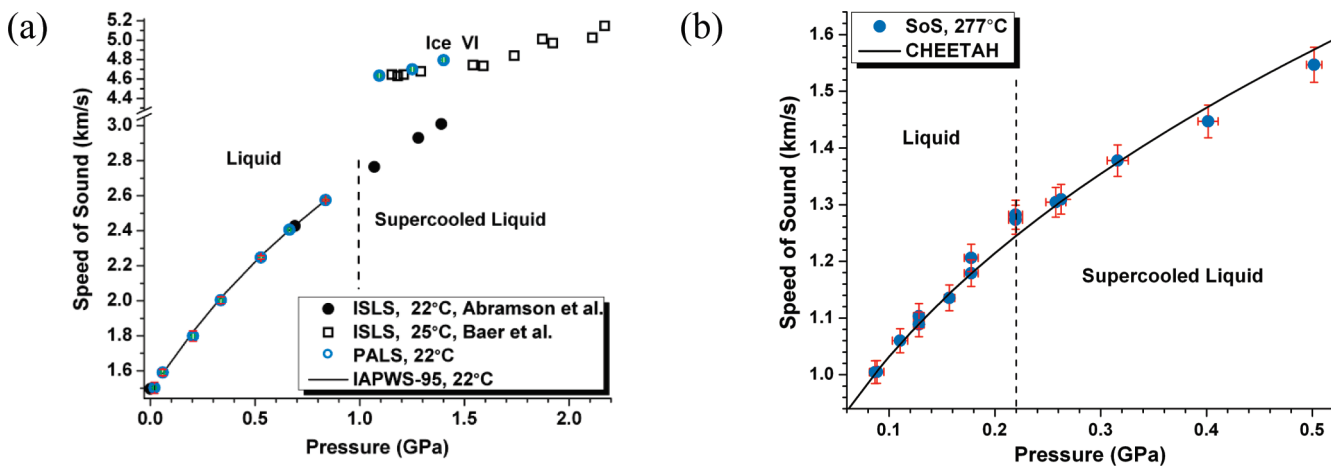


Figure 4. (a) Determination of the collection wavevector, K_S , is accomplished by measuring acoustic frequency, ν_A , from a sample with a known c . Here K_S is determined using the velocity for water at 0.66 GPa, 22 °C, from the 1995 International Association for the Properties of Water and Steam, (IAPWS-95); red error bars indicate percent differences between PALS and IAPWS-95 velocity values, and green error bars (smaller in dimension than the corresponding open circle plot symbol) indicate the shift in pressure before and after each velocity measurement.²⁰ PALS water results, anchored by the 0.66 GPa calibration point, compare well with measurements of liquid- and solid-state H_2O made by Abramson et al. and Baer et al.^{14,21} (b) Experimental sound velocity data from HBO_2 (liq.), filled blue circles; and calculated velocities using an EXP6-polar function, solid line. Red error bars indicate $\pm 2\%$ of each sound velocity value and the change in pressure before and after each speed of sound measurement.

radiation also diffracts from the traveling wave, generating a diffracted field, E_D ($I_D = E_D^2$), with a time-varying phase. Two pinhole apertures are positioned behind the DAC to select a signal collection wavevector, K_S , and pass a narrow cone of light ($<1 \times 10^{-4}$ % of the available DAC solid angle) to a photomultiplier tube (PMT). Signal intensity measured at the PMT is equal to the square of the mixed fields (heterodyne detection) and is modulated by the time-varying optical phase difference between E_R and E_D .¹⁹ Here the frequency of the material response is given by $\nu_A = 2c/\lambda_P(\sin \theta/2)$, where c is the adiabatic speed of sound, λ_P is the probe wavelength, and θ is equal to the probe angle of incidence, θ_{Pi} , plus the probe angle of diffraction, θ_{Pd} . (See the Supporting Information for additional experimental details.)

Time-domain series (Figure 3b) are Fourier transformed to compute modulation frequencies ($\nu_A < 2$ GHz for $\theta = 10^\circ$, $c \leq 6$ km/sec, $\lambda_P = 532$ nm). The use of a single Pt strip and a cylindrical probe-pulse profile increases the number of modulations in the T-D series and enables more precise determinations of acoustic frequency. Physical disparities on Pt strips with dimensions on the scale of the probe wavelength enable LO signal to be diffracted along K_S . An animation of the PALS process is available. (See the Supporting Information.). The value of K_S is determined by conducting several acoustic frequency measurements of water, at a fixed pressure and temperature. Accurate water $c(P,T)$ literature data are used in combination with the measured frequency to determine K_S (3467.8 cm^{-1}), a value that is then used to determine all subsequent high P-T sound velocities from materials encapsulated by the same DAC. If diamond anvils are changed or new sample container window materials are inserted, then K_S is recalibrated. PALS measurements from water compare favorably to the well-established IAPWS-95 formulation including accurate ISLS results (Figure 4a).^{14,20,21} The 1σ standard deviation (Gaussian distribution) of % c variation across

14 fixed P-T measurements at 0.66 GPa and 22 °C made at vastly different regions within the DAC sample chamber is 0.77 %. Speeds of sound are determined by $c = \nu_A/K_S$. The reproducibility of PALS measurements is dependent on the DAC alignment to the incoming probe pulse and the physical stability of the optical system and DAC. (See the Supporting Information.) The precision of pressure determinations, using the $SrB_4O_7:\text{Sm}^{2+}$ optical manometer, is stated to be 0.02 GPa from 22 to 450 °C.¹⁴

The molecular stability of HBO_2 was verified by μ -FTIR up to 277 °C and 0.7 GPa. At 277 °C and above 0.22 GPa, HBO_2 begins to slowly freeze. In this pressure range, the interpolated melting curve is relatively steep, 490 °C/GPa. Above 300–350 °C, and after ~60 min, the optical manometer material ($SrB_4O_7:\text{Sm}^{2+}$) employed to determine sample pressure consistently failed to fluoresce. The narrow $P-T$ region where fluid-state HBO_2 measurements are accessible may explain the lack of any previous data. Sound velocity results for HBO_2 (liq.) are plotted in Figure 4b.

Adiabatic sound velocity data were used to parametrize HBO_2 product intermolecular interaction potentials, thus enabling accurate predictions of thermodynamic and chemical equilibrium states of highly energetic reactions involving boron-containing or loaded compounds. To this end, we employ an EXP6-polar thermodynamics theory that was previously shown to yield very good results for the properties of hot, dense water as well as those of HNO_2 .^{22,23} HBO_2 is also a strongly polar molecule with a dipole moment larger than H_2O ; for the purpose of modeling HBO_2 , we set the value of its dipole moment to the calculated value for the isolated molecule, $\mu = 2.78$ D.²⁴ It is possible and quite likely that similarly to H_2O a somewhat larger value of μ may be more appropriate for describing HBO_2 under the high density fluid conditions typical of detonation or high-pressure combustion. However, the limited experimental data presently available do not

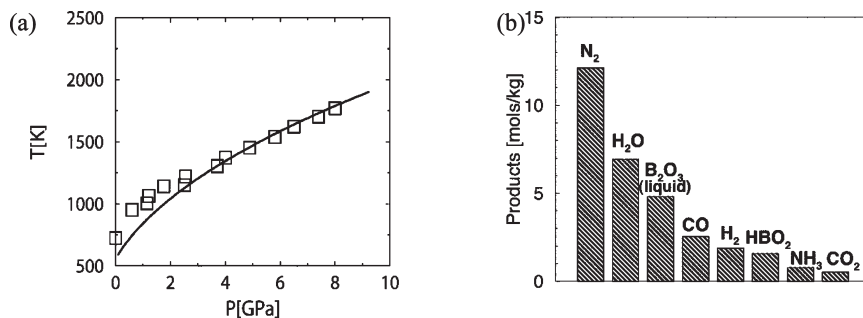


Figure 5. (a) Calculated B₂O₃ melt curve from CHEETAH (solid line) compared with experimental data (open squares) from Brazhkin et al.³³ (b) Calculated C–J plane decomposition mixture from 70% tetrinitromethane + 30% borazine (B₃N₃H₆).

warrant trying to discern such an effect; we expect that this approximation will have little effect on our conclusions regarding the character of detonations containing boron, which at this point can only be largely qualitative. We find that EXP6 parameter values, $r_0 = 3.976 \text{ \AA}$, $\varepsilon = 216.3 \text{ K}$, and $\alpha = 12.67$, using the above dipole moment yield good agreement with the sound velocity measurements; see Figure 4. Thermodynamic calculations using these parameters place the critical point of HBO₂ approximately at $T_c = 447 \text{ }^\circ\text{C}$ and $P_c = 260 \text{ atm}$; of course, chemical reactivity may actually intervene before these conditions can be reached.

The important role that molecular HBO₂ is likely to play in hydrocarbon or organometallic explosive combustion of boron particles (e.g., in rocket propellants and ramjet fuels) is well-documented.^{9,11,25–29} Here we attempt to quantify its impact in the detonation of explosives containing elemental boron by employing the newly determined HBO₂ thermodynamics in the calculation of detonation velocities. These calculations are performed using the thermochemical code CHEETAH and are similar to those described, for example, in ref 30. The code is used here to determine C–J points of explosives. Detonation product results are constrained to single-phase fluid mixtures and, potentially, many condensed phases, all in chemical equilibrium. The major boron-containing products likely to be relevant for such processes have been discussed, for example, by Akimov et al.³¹ The fluid phase components we consider are small molecular products such as N₂, CO₂, H₂O, CO, NH₃, CH₄, HBO₂, O₂, H₂, and so on, which are thermodynamically favored at high temperatures and pressures; they are all modeled by EXP6 or EXP6-polar interactions and tested favorably against experimental data. The condensed phases are carbon (diamond and graphite), B₂O₃ (liquid and solid), B (solid and liquid), BN (cubic and hexagonal solids), CB₄ (solid), and H₃BO₃ (solid), all described by Murnaghan-type EOS that reproduce available high-pressure experimental results. Among these, B₂O₃ is of particular importance; it is likely the oxidation endpoint of boron. Unfortunately, B₂O₃ experimental data are very scarce and in fact nonexistent for the liquid phase. We note however that our liquid EOS is in good agreement with the simulation results of Ohmura et al., and the melting line agrees well with that reported by Brazhkin et al. (Figure 5a).^{32,33} Nevertheless, such uncertainties due to the lack of EOS data for likely major reaction products probably limit our ability to make fully

quantitative predictions. The combustion of solid boron particles is plagued by well-known kinetics issues, which are likely to also be important in the detonation of explosives loaded with metallic boron, just as in the case of aluminum-loaded compositions.³⁴ We attempt to circumvent these complications and focus therefore on explosive mixtures with boronated organic compounds, which were studied experimentally.³² These are, (1) 86% (by weight) pentaerythritol tetrinitrate (C₅H₈N₄O₁₂) + 14% orthocarborane (C₂B₁₀H₁₂), (2) 75% tetrinitromethane (CN₄O₈) + 25% pentaborane (B₅H₉), and (3) 70% tetrinitromethane + 30% borazine (B₃N₃H₆); their initial densities are $\rho_0 = 0.78, 1.14$, and 1.28 g/cm³, respectively. The experimental detonation velocities reported are $D_{\text{exptl}} = 4.64, 5.9$, and 6.3 km/s; our corresponding calculated values are $D_{\text{calcd}} = 4.78$ ($\Delta = 3.02\%$), 5.96 ($\Delta = 1.02\%$) and 6.13 ($\Delta = -2.70\%$) km/s, respectively, indicating reasonable agreement. For these energetic mixtures, we find that the major detonation products containing boron are HBO₂ and B₂O₃ (liq.) (mixture 2 also yields a small amount of liquid boron), mixed with the molecular detonation products typical for CHNO-type explosives. We show for example in Figure 5b the C–J region composition of mixture number three, which indicates, as expected, that large amounts of water also result upon detonation. Because the reaction of B₂O₃ (liq.) with water is likely an important route toward the formation of HBO₂, its study at high temperatures and pressures will significantly increase the confidence of quantitative predictions of the thermodynamic and kinetic behavior of boron-containing explosives and propellants.¹⁰

We emphasize that the HBO₂ sound speed measurements provide essential input for its EOS and the thermochemical calculations. We note, for example, that assuming that HBO₂ is identical to water (perhaps a “reasonable” guess in the absence of experimental or theoretical evidence) leads to differences of 3–15% in the detonation velocities of the above explosives. Such differences can increase only when the amount of boron present is larger because the chemical equilibrium is sensitive to HBO₂ modeling.

Previously, accurate sound velocity measurements of highly photosensitive materials were hindered by the necessity to use relatively high-fluence pulsed laser systems. Moreover, established T-D techniques, which are optimal for determining EOSs of liquid materials, require >25–30 μm thick samples. We expect that the relative simplicity and high versatility of PALS-type measurements will assist research

initiatives directed to understand a wide-array of extreme condition chemical processes. Here we conducted sound velocity measurements on a rather challenging material and, in turn, the $\text{HBO}_2(\text{liq.})$ data enable semiempirical EOS-based thermochemical modeling of high-pressure combustion, deflagration, and detonation chemistry involving boron with a reasonable level of confidence. Our study reveals that HBO_2 is an important detonation product for boron-containing explosives and suggests that the reaction of $\text{B}_2\text{O}_3(\text{liq.}) + \text{H}_2\text{O}$ (supercritical) is a plausible route toward the formation of HBO_2 under detonation conditions. We also note that in situations where a carbon deficient oxidizer, for example, ammonium perchlorate (NH_4ClO_4), reacts with 10 wt % boron, our calculations predict that up to five times more HBO_2 product is likely to be found compared with the boron-containing explosives previously discussed: a reasonable result given that the concentration of oxygen competing carbon products, for example, CO and CO_2 , is severely diminished.

SUPPORTING INFORMATION AVAILABLE QuickTime animation of the PALS sequence, a description of the FIB Pt deposition procedure, and PALS experimental layout details. This material is available free of charge via the Internet at <http://pubs.acs.org>.

AUTHOR INFORMATION

Corresponding Author:

*To whom correspondence should be addressed. E-mail: zaug1@llnl.gov.

ACKNOWLEDGMENT J.M.Z. is grateful to L. E. Fried, J. M. Brown, and E. H. Abramson for stimulating and thoughtful discussions. We thank E. H. Abramson for providing single crystals of $\text{SrB}_4\text{O}_7:\text{Sm}^{2+}$ and Kwei-Yu Chu for creating the PALS animation sequence. This research was supported by the DOE Campaign-II and Joint DoD/DOE Munitions Technology Programs and performed under the auspices of the U.S. Department of Energy by Lawrence Livermore National Laboratory under contract DE-AC52-07NA27344.

REFERENCES

- (1) Drake, M. J.; Richter, K. Determining the Structure of the Earth. *Nature* **2002**, *416*, 39–44.
- (2) Bergeron, P.; Saumon, D.; Wesemael, F. New Model Atmospheres for Very Cool White Dwarfs with Mixed H/He and Pure He Compositions. *Astrophys. J.* **1995**, *443*, 764–779.
- (3) Cavazzoni, C.; Chiarotti, G. L.; Scandolo, S.; Tosatti, E.; Bernasoni, M.; Parrinello, M. Superionic and Metallic States of Water and Ammonia at Giant Planet Conditions. *Science* **1999**, *285*, 44–46.
- (4) Koshizuka, S.; Ikeda, H.; Oka, Y. Numerical Analysis of Fragmentation Mechanisms in Vapor Explosions. *Nucl. Eng. Des.* **1999**, *189*, 423–433.
- (5) Clupara, D.; Lyubovsky, M. R.; Altman, E.; Pfefferle, L. D.; Datye, A. Catalytic Combustion of Methane over Palladium-Based Catalysts. *Cat. Rev.-Sci. and Eng.* **2002**, *44*, 593–649.
- (6) Fickett, W.; Davis, W. C. Detonation Theory and Experiment; Dover Publications: Mineola, NY, 1979.
- (7) Albenze, E. J.; Thompson, M. O.; Clancy, P. Molecular Dynamics Study of Explosive Crystallization of SiGe and Boron-Doped SiGe Alloys. *Ind. Eng. Chem. Res.* **2006**, *45*, 5628–5639.
- (8) Cook, M. A.; Filler, A. S.; Keyes, R. T.; Partridge, W. S.; Ursenbach, W. O. Aluminized Explosives. *J. Chem. Phys.* **1957**, *61*, 189–196.
- (9) Peretz, A. Some Theoretical Considerations of Metal-Fluorocarbon Compositions for Ramjet Fuels. *Proceedings of the Eighth International Symposium on Air Breathing Engines*, Cincinnati, OH, June 14–19, 1987; Billig, F. S., Ed.; American Institute of Aeronautics and Astronautics, Inc.: New York; pp 398–403.
- (10) Foelsche, R. O.; Burton, R. L.; Krier, H. Boron Particle Ignition and Combustion at 30–150 ATM. *Combust. Flame* **1999**, *117*, 32–58.
- (11) Meschi, D. J.; Chupka, W. A.; Berkowitz, J. Heterogeneous Reactions Studied by Mass Spectrometry. I. Reaction of $\text{B}_2\text{O}_3(\text{s})$ with $\text{H}_2\text{O}(\text{g})$. *J. Chem. Phys.* **1960**, *33*, 530–532.
- (12) Yan, Y.-X.; Nelson, K. A. Impulsive Stimulated Light Scattering. II. Comparison to Frequency-Domain Light-Scattering Spectroscopy. *J. Chem. Phys.* **1987**, *87*, 6257–6265.
- (13) Zaug, J. M.; Slutsky, L. J.; Brown, J. M. Equilibrium Properties and Structural Relaxation in Methanol to 30.4 GPa. *J. Phys. Chem. B* **1994**, *98*, 6008–6016.
- (14) Abramson, E. H.; Brown, J. M. Equation of State of Water Based on Speeds of Sound Measured in the Diamond-Anvil Cell. *Geochim. Cosmochim. Acta* **2004**, *68*, 1827–1835.
- (15) Lin, H. -N.; Stoner, R. J.; Maris, H. J.; Tauc, J. Phonon Attenuation and Velocity Measurements in Transparent Materials by Picosecond Acoustic Interferometry. *J. Appl. Phys.* **1991**, *69*, 3816–3822.
- (16) Pezeril, T.; Ruello, P.; Gougeon, S.; Chigarev, N.; Mounier, J. M.; Picart, P.; Gusev, V. Generation and Detection of Plane Coherent Shear Picosecond Acoustic Pulses by Lasers: Experiment and Theory. *Phys. Rev. B* **2007**, *75*, 174307.
- (17) Kou, C.-Y.; Vieira, M. M. F.; Patel, C. K. N. Transient Optoacoustic Pulse Generation and Detection. *J. Appl. Phys.* **1984**, *55*, 3333–3336.
- (18) *Physical Acoustics*; Mason, W. P., Thurston, R. N., Eds.; Academic Press: New York, 1988; Vol. XVIII.
- (19) Crimmons, T. F.; Stoyanov, N. S.; Nelson, K. A. Heterodynied Impulsive Stimulated Raman Scattering of Phonon-Polaritons in LiTaO_3 and LiNbO_3 . *J. Chem. Phys.* **2002**, *117*, 2882–2896.
- (20) Wagner, W.; Prüß, A. The IAPWS Formulation 1995 for the Thermodynamic Properties of Ordinary Water Substance for General Scientific Use. *J. Chem. Ref. Data* **2002**, *31*, 387.
- (21) Baer, B. J.; Brown, J. M.; Zaug, J. M.; Schiferl, D.; Chronister, E. L. Impulsive Stimulated Scattering in Ice VI and Ice VII. *J. Chem. Phys.* **1997**, *108*, 4540–4544.
- (22) Bastea, S.; Fried, L. E. Exp6-Polar Thermodynamics of Dense Supercritical Water. *J. Chem. Phys.* **2008**, *128*, 17502.
- (23) Maiti, A.; Bastea, S.; Howard, W. M.; Fried, L. E. Nitrous Acid under High Temperature and Pressure – from Atomistic Simulations to Equations of State for Thermochemical Modeling. *Chem. Phys. Lett.* **2009**, *468*, 197–200.
- (24) Dewar, M. J. S.; Jie, C. X.; Zoebisch, E. G. AM1 Calculations for Compounds Containing Boron. *Organometallics* **1988**, *7*, 513–521.
- (25) Macek, A.; Semple, J. M. Combustion of Boron Particles at Atmospheric Conditions. *Combust. Sci. Technol.* **1969**, *1*, 181–191.
- (26) Yetter, R. A.; Rabitz, F. L.; Dryer, F. L.; Brown, R. C.; Kolb, C. E. Kinetics of High-Temperature B/O/H/C Chemistry. *Combust. Flame* **1991**, *83*, 43–62.
- (27) Ulas, A.; Kuo, K.; Gotzmer, G. Ignition and Combustion of Boron Particles in Fluorine-Containing Environments. *Combust. Flame* **2001**, *127*, 1935–1957.

- (28) Spalding, M. J.; Krier, H.; Burton, R. L. Boron Suboxides Measured during Ignition and Combustion of Boron in Shocked Ar/F/O₂ and Ar/N₂/O₂ Mixtures. *Combust. Flame* **2000**, *120*, 200–210.
- (29) Sullivan, K.; Young, G.; Zachariah, M. R. Enhanced Reactivity of Nano-B/Al/CuO MIC's. *Combust. Flame* **2009**, *156*, 302–309.
- (30) Scott, H. P.; Hemley, R. J.; Mao, H. K.; Herschbach, D. R.; Fried, L. E.; Howard, W. M.; Bastea, S. Generation of Methane in the Earth's Mantle: In Situ High Pressure-Temperature Measurements of Carbonate Reduction. *Proc. Natl. Acad. Sci. U.S.A.* **2004**, *101*, 14023–14026.
- (31) Akimov, L. N.; Apin, A. Ya.; Stesik, L. N. Detonation of Explosives Containing Boron and Its Organic Derivatives. *Combust., Explos. Shock Waves (Engl. Transl.)* **1972**, *8*, 387–390.
- (32) Ohmura, S.; Shimojo, F. Anomalous Pressure Dependence of Self-Diffusion in Liquid B₂O₃: an Ab Initio Molecular Dynamics Study. *Phys. Rev. B* **2009**, *80*, 020202(R).
- (33) Brazhkin V. V.; Katayama Y.; Inamura Y.; Kondrin M. V.; Lyapin A. G.; Popova S. V; Voloshin R. N. Structural Transformations in Liquid, Crystalline, and Glassy B₂O₃ under High Pressure [JETP Lett. 78 (6), 393–397 (2003)]. *JETP Lett.* **2004**, *79*, 308.
- (34) Young, G.; Sullivan, K.; Zachariah, M. R.; Yu, K. Combustion Characteristics of Boron Nanoparticles. *Combust. Flame* **2009**, *156*, 322–333.